

**Experiments and characterization of low-frequency oscillations in a granular column**Loreto Oyarte Gálvez,<sup>1,\*</sup> Nicolás Rivas,<sup>2</sup> and Devaraj van der Meer<sup>1</sup><sup>1</sup>*Physics of Fluids, Universiteit Twente, P. O. Box 217, 7500AE Enschede, The Netherlands*<sup>2</sup>*Forschungszentrum Jülich GmbH, Helmholtz-Institut Erlangen-Nürnberg für Erneuerbare Energien (IEK-11), Dynamik komplexer Fluide und Grenzflächen, Fürther Straße 248, 90429 Nürnberg, Germany*

(Received 27 October 2017; published 11 April 2018)

The behavior of a vertically vibrated granular bed is reminiscent of a liquid in that it exhibits many phenomena such as convection and Faraday-like surface waves. However, when the lateral dimensions of the bed are confined such that a quasi-one-dimensional geometry is formed, the only phenomena that remain are bouncing bed and the granular Leidenfrost effect. This permits the observation of the granular Leidenfrost state for a wide range of energy injection parameters and more specifically allows for a thorough characterization of the low-frequency oscillation (LFO) that is present in this state. In both experiments and particle simulations we determine the LFO frequency from the power spectral density of the center-of-mass signal of the grains, varying the amplitude and frequency of the driving, the particle diameter, and the number of layers in the system. We thus find that the LFO frequency (i) is inversely proportional to the fast inertial timescale and (ii) decorrelates with a typical decay time proportional to the slow dissipative timescale in the system. The latter is consistent with the view that the LFO is driven by the inherent noise that is present in the granular Leidenfrost state with a low number of particles.

DOI: [10.1103/PhysRevE.97.042901](https://doi.org/10.1103/PhysRevE.97.042901)**I. INTRODUCTION**

Granular materials are observed on a daily basis; they are present in many natural phenomena such as avalanches, landslides, or the formation of dunes, and they have a wide range of applications [1]. The exploration of the similarities between the behavior of granular materials and that of ordinary fluids has motivated much appealing research. An important example is a vertically shaken granular bed, which exhibits fluidlike behavior [2] that in turn depends, in part, on the injected energy, the number of particle layers, and the system geometry. As the shaking energy is increased, the system transits from (i) a bed of grains bouncing with the base to (ii) bursts; (iii) undulations [3–7] (which are analogous to Faraday waves in regular liquids [8,9]); (iv) density inversion [10–12], where a dense layer of grains floats on top of a gaseous layer, a state referred to as the Leidenfrost state due to its similarity to a liquid droplet floating on its own vapour above a hot plate [13]; (v) buoyancy driven convection rolls [14,15] and, for very high shaking energy, to (vi) a granular gas (a dilute granular system with particles moving randomly throughout the container).

For a sufficiently large number of particle layers the granular bed transits from the Leidenfrost state to the convection state as the energy input is increased. Recently, an oscillation was observed in the motion of the dense part of the Leidenfrost state [16,17]. The frequency of these oscillations is typically much lower than the frequency of the injected energy and becomes dominant in the dynamics of the system when the energy input increases. Recently, these so-called low-frequency oscillations (LFO) were indirectly observed in a

three-dimensional vibrofluidized granular bed by tracing the movement of a single particle through the bulk using positron emission particle tracking [18], showing a good agreement with numerical simulations, where the effect was first observed [16].

How the above fluidlike behaviors in a granular bed depend on the container's geometry can be represented in a phase diagram, as shown in Fig. 1 [16]. Here the occurrence of the phenomena is schematically indicated as a function of the container width and the energy injection. When the container is large enough (larger than approximately 20 particle diameters) and filled with a sufficiently large amount of particles, the system can exhibit any of the above-mentioned behaviors depending on the energy injection parameters. But for narrower containers many of these phenomena are suppressed by the geometry of the container, since bursts, undulations, and convection rolls are extended in the horizontal direction. These patterns are frustrated by the presence of the side walls, which can be attributed to, e.g., effective viscosity and lateral heat conduction [19]. Therefore, in a quasi-one-dimensional container only the bouncing bed and Leidenfrost states are present.

The possibility to keep the system in the Leidenfrost regime by using a narrow container and thus observe LFO's for a wide range of shaking strengths has motivated this work. We experimentally study the behavior of the LFO's and their role in the dynamics of the system. The results are compared with simulations showing a very good agreement between both. Moreover, we analyze the timescales present in the system and relate them to the LFO frequency, finding that when using suitable dimensionless quantities the LFO frequencies collapse onto a single curve independent of the number of layers and particle diameter. Finally, we analyze the strength of the LFO by describing the system by means of a Langevin

\*l.a.oyartegalvez@utwente.nl

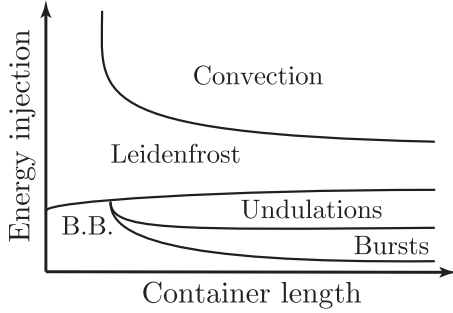


FIG. 1. Schematic phase diagram of a vibrated quasi-two-dimensional granular bed as a function of the energy injection and the container's length. Here, B.B. indicates the bouncing bed state and the granular gas state is reached for very high energy injection which lies outside the range of the phase diagram.

equation of a noise-driven harmonic oscillator. We find that the measured LFO's strength and the strength scaling derived from the Langevin equation are consistent, and we show that the energy equipartition is increasingly violated with the increment of the shaking strength.

This article is organized as follows. In Sec. II, the experimental setup and the simulations are detailed. In Sec. III, we analyze the experimental results and compare them to the simulations; in addition the different timescales presented in the system are explained and analyzed. Finally, in Sec. IV a summary of this study is presented.

## II. SYSTEM DESCRIPTION

### A. Experimental setup

The experimental setup consists of a quasi-one-dimensional transparent acrylic container, with base dimensions ( $L_X$ ,  $L_Y$ ) much smaller than the height (height  $\times L_X \times L_Y = 150 \times 5 \times 5 \text{ mm}^3$ ), as shown in Fig. 2(a). The container is partially filled with monodispersed stainless steel beads of three different diameters,  $d = 0.5, 1.0, \text{ and } 2.5 \text{ mm}$ , i.e., the container width  $L = L_X = L_Y$  corresponds to  $L = 10d, 5d, \text{ and } 2d$ , respectively. The system is mounted on a sinusoidally vibrating

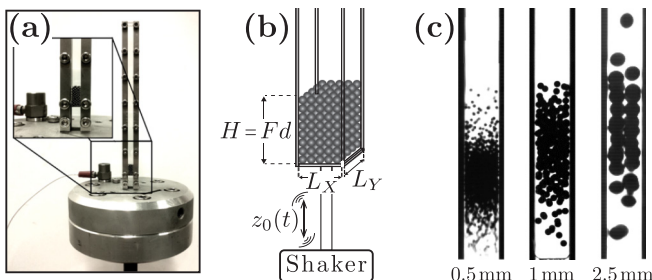


FIG. 2. (a) A full picture and a zoomed-in view of the experimental setup: The container is mounted on top of the mechanical shaker, with the bottom located at approximately 1 cm above the socket. Note that the granular material above it is at rest. (b) A schematic of the container, where the dimensions of the container and the filling height  $H$ , related to the filling factor  $F$  and particle diameter  $d$ , are indicated. (c) Typical images of the partially filled container under shaking for the three different particle diameters,  $d = 0.5, 1.0, 2.5 \text{ mm}$ .

TABLE I. Experimental parameters, the shaker amplitude  $a_0$ , its frequency  $f_0$ , the diameter of the particles  $d$ , and the number of particle layers  $F$  used in the experiment.

$a_0$ (mm)	$f_0$ (Hz)	$d$ (mm)	$F$
1, 2, 3, 4	40–110	0.5, 1, 2.5	8, 12, 16

electromechanical shaker with tuneable frequency  $f_0$  and amplitude  $a_0$ , i.e., the vertical position of the bottom is given by

$$z_0(t) = a_0 \sin(2\pi f_0 t). \quad (1)$$

Front view images are obtained using a high-speed camera capturing 500 frames per second during 2 min; examples for every particle size are shown in Fig. 2(c). For every set of parameters 5 to 10 acquisitions were performed, in order to reduce the statistical error.

Two dimensionless numbers have been previously found to be relevant in the Leidenfrost state [10], which we choose as control parameters: (i) the number of monolayers at rest  $F = Nd^2/L^2$ , with  $N$  the total number of particles, and (ii) the dimensionless shaking strength  $S = (2\pi a_0 f_0)^2/g\ell$ , where  $\ell$  corresponds to the typical displacement of the particles and  $g$  is the gravitational acceleration. Both dimensionless numbers,  $F$  and  $S$ , are varied by changing the parameters  $a_0$ ,  $f_0$ ,  $N$ , and  $d$ . The experimental parameters used in this study are summarized in Table I.

In Fig. 3(a), a sequence of images shows the system in the Leidenfrost regime, where a dense volume of grains is seen to float over a much less dense gaseous layer. From the images it is not possible to obtain the position of all the particles as it is not feasible to distinguish individual particles for such high densities. Therefore, in order to obtain the vertical coordinate of the center of mass ( $z_{CM}$ ) we compute the horizontal intensity average of every image, obtaining a vertical density profile at each point in time, as shown in Fig. 3(b). We then define the vertical positions of the center of mass  $z_{CM}(t)$  of the granular bed as that of the center of mass of the density profile at each individual point in time [cf. Figs. 3(b) and 3(c)]. To verify this

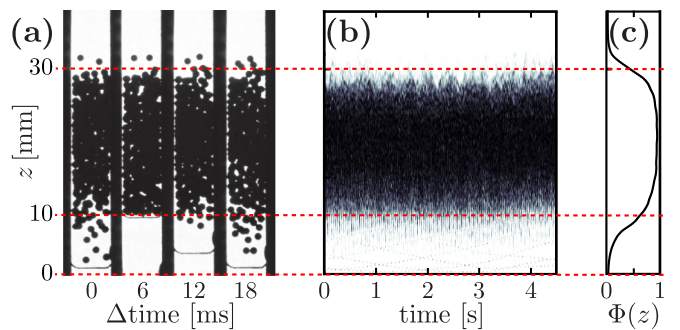


FIG. 3. (a) A sequence of images of the system in different phases of the driving showing a dense cluster floating over a dilute, gaseous granular layer. This sequence corresponds to one period of oscillation of the shaker. (b) Average of the black and white pixels on every horizontal level for each frame as a function of time, referred to as density profile. (c) Time-averaged density profile of the system.

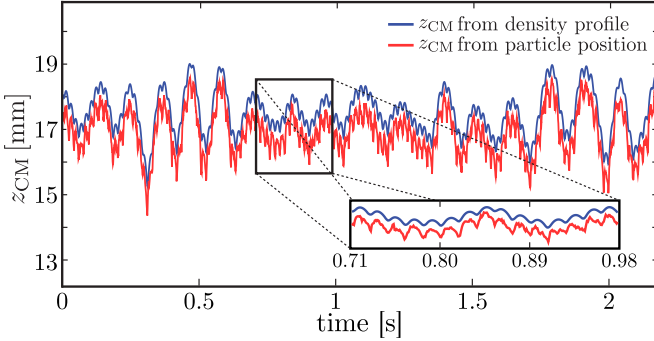


FIG. 4. A comparison of the vertical position of the center of mass  $z_{\text{CM}}(t)$  computed directly from the position of the particles (blue line) and using the experimental method, i.e., from the density profile (red line); data obtained using numerical simulations. The frequency that dominates the main plot corresponds to that of the LFO, whereas in the region that is magnified in the inset the driving frequency  $f_0$  can also be appreciated.

procedure we use data from numerical simulations (detailed further below) to compute the  $z_{\text{CM}}(t)$  using two approaches: (i) from the exact position of the particles and (ii) from the density profile as done in experiments. As shown in Fig. 4, there is a quite good agreement in the computed  $z_{\text{CM}}(t)$  using both approaches. However, the density profile approach consistently overpredicts  $z_{\text{CM}}(t)$  since it does not differentiate between a single particle in the gaseous regime and a series of particles stacked in the  $y$  direction in the dense region. Nonetheless, the frequency of oscillation of the  $z_{\text{CM}}(t)$  is accurately captured.

### B. Simulations

Simulations are performed using event-driven (ED) molecular dynamics [20]. Particles are considered as hard spheres, which implies binary collisions, no overlap, and no long-range forces between them. Collisions are modelled by normal and tangential velocity-dependent restitution coefficients, following the expression in Ref. [21]. This is the same simulation code used in the original study of LFO [16], where a more detailed description of the algorithm can be found. Material properties were chosen such that, at a typical particle velocity  $\bar{v} = 0.3$  m/s, the relevant coefficient of restitution is  $\bar{r} = 0.93$  for both particle-particle and particle-wall collisions. Velocity-dependent  $\bar{r}$  ensures that dissipation is not overestimated at high particle densities, as can occur when using constant coefficients [22]. Static and dynamic friction coefficients ( $\mu_s$  and  $\mu_d$ , respectively) are also considered and held constant at  $\mu_s = \mu_d = 0.08$  also for both types of collisions. In general, variation of these parameters influences the values of the measured quantities (as will be discussed later), but the qualitative aspects remain the same, even if periodic boundary conditions are used and friction is set to zero. These particular values of  $\mu$  and  $\varepsilon$  were taken as fitting parameters to obtain a good agreement with the experimental data and are in the range of measured values for millimetric stainless steel spheres.

### C. Shaking strength

The definition of the typical particle displacement  $\ell$ , and hence the dimensionless shaking strength  $S$ , is not straight-

forward, since it sensitively depends on the system state. When the granular bed is only slightly fluidized the typical displacement is highly correlated with the shaking amplitude, therefore  $\ell = a_0$  is a good approximation, and the shaking strength becomes the dimensionless acceleration

$$S_{a_0} = \Gamma = \frac{a_0(2\pi f_0)^2}{g}. \quad (2)$$

On the other hand, when the granular bed is strongly fluidized this length scale is decoupled from the shaking amplitude  $a_0$  and therefore an intrinsic parameter, namely the particle diameter  $\ell = d$ , becomes a more sensible choice [2,10,23]. With this choice, the dimensionless shaking strength becomes

$$S_d = \frac{(2\pi a_0 f_0)^2}{d g}. \quad (3)$$

For states with a high energy injection rate, such as the Leidenfrost regime, where it is clearly observed that particles near the bottom typically travel distances which are larger than the shaking amplitude,  $S_d$  appears as the proper dimensionless parameter to describe such a driven system (as long as the particle diameter  $d$  is kept constant), as confirmed by experiments and a theoretical hydrodynamic model [2]. In the following section, we will, however, see that in our case, where  $d$  is actually varied, we will need to reconsider the choice of the dimensionless control parameter.

## III. ANALYSIS OF RESULTS

The granular Leidenfrost state is an example of spontaneous segregation or symmetry breaking where an initially homogeneous, monodisperse granular material separates into a dense and a dilute region. This is the result of interparticle collisions being dissipative and of a stochastic nature [24–27]. More specifically, in the granular Leidenfrost state a dense, liquidlike, or even almost solidlike cluster is floating on top of a dilute, gaseous region. Such a system is analogous to a piston (the cluster) that encloses an amount of gas. Since the piston is free to move up and down, the enclosed gas responds as a spring: When the cluster moves down, it is compressed and tries to push the cluster upwards, thereby trying to restore the equilibrium situation. Clearly, when the cluster moves upwards, the gas expands, the force on the cluster decreases, and the equilibrium is again restored. Qualitatively, this is the phenomenon that lies at the basis of the LFO. As mentioned before, and as was observed in previous works [16–18], by studying a quasi-one-dimensional geometry most of the phenomena in the rich phase diagram can be suppressed, leaving only the bouncing bed and Leidenfrost state to develop. This allows us to directly observe these collective oscillations of the particles in a relatively large parameter window. In this section we will first study how the frequency  $f_{\text{LFO}}$  of the Leidenfrost oscillation depends on the parameters of the system, where we predominantly vary the particle size  $d$ , the filling factor  $F$  and the dimensionless shaking strength  $S_d$ . From an analysis of the relevant timescales in the system we subsequently determine a natural scaling for  $f_{\text{LFO}}$  and show that with an appropriate choice of dimensionless parameters the data can be made to collapse onto a single curve. Subsequently, we study the

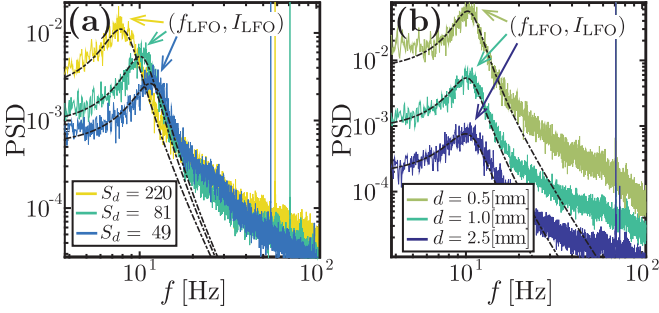


FIG. 5. The PSD of the time evolution of the center of mass  $z_{\text{CM}}(t)$  for (a) different shaking strengths  $S_d$  with constant particle diameter  $d = 1$  mm and (b) different particle diameters  $d$  with constant shaking strength  $S_d = 81$ , obtained from experimental data for  $F = 12$ . The LFO is clearly distinguished as a broad peak around the 10-Hz region and its frequency  $f_{\text{LFO}}$  can be determined from the location of the peak's maximum. The black dashed lines represent theoretical results calculated from the Langevin model [Eq. (11)].

coherence time and the amplitude of the oscillation and show that the mechanism that drives the LFO is connected to the stochastic character of the system.

### A. LFO frequency

As can be seen in Fig. 4, the time evolution of the center of mass  $z_{\text{CM}}(t)$  shows oscillations with two clearly distinct frequencies: a fast one, corresponding to the frequency of the shaker  $f_0$ , and a much slower one,  $f_{\text{LFO}}$ , which corresponds to the low-frequency Leidenfrost oscillations. To determine this last frequency, we compute the power spectral density (PSD) of  $z_{\text{CM}}(t)$ , shown in Fig. 5 for (a) different shaking strengths  $S_d$  and (b) different particle diameters  $d$ . The frequency from the shaker  $f_0$  and its harmonics are immediately recognized as well-defined, narrow peaks in the PSD. In addition, there is an equally clear wide and shallow peak, which corresponds to the LFO. Surprisingly, the frequency  $f_{\text{LFO}}$  decreases when the injected energy increases; in other words, the typical period of the collective oscillation of the system is larger when the injected energy increases. Furthermore, the peak corresponding to the LFO becomes narrower and higher with increasing injected energy and with decreasing particle diameter. This suggests that this collective behavior becomes more coherent in time as  $S_d$  increases and  $d$  decreases.

The  $f_{\text{LFO}}$  was determined from the PSD as a function of the driving strength  $S_d$  for different numbers of layers  $F$  and particle diameters  $d$ , the result of which is shown in Figs. 6(a) and 6(b), respectively. The plot contains both experimental (closed symbols) and numerical (open symbols) data, where the different symbols correspond to different values of the vibration amplitude  $a_0$ . The fact that the data collapse irrespective of the value of  $a_0$  proves that  $f_{\text{LFO}}$  indeed only depends on the combination  $S_d$  and not on  $a_0$  and  $f_0$  separately. Our data are consistent with the scaling proposed by Rivas *et al.* [16], namely  $f_{\text{LFO}}(S_d) \sim S_d^{-\alpha}$ , with  $\alpha \approx 0.3$ .

### B. A simple model for the LFO

A key question we want to address is as follows: How does the frequency of the LFO scale with the parameters in the

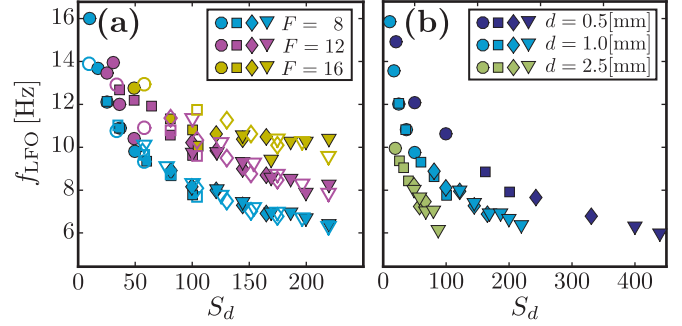


FIG. 6. The LFO frequency  $f_{\text{LFO}}$  is plotted versus the dimensionless shaking strength  $S_d$  for (a) different numbers of layers  $F$  and a constant particle diameter  $d = 1$  mm, and (b) different particle diameters and a constant number of layers  $F = 8$ . The different symbols correspond to different amplitudes of the shaker,  $\circ = 1.0$  mm,  $\square = 2.0$  mm,  $\diamond = 3.0$  mm,  $\nabla = 4$  mm. The solid symbols represent experimental data and the open symbols numerical simulation results.

system? We find an answer by turning to a highly simplified mass-spring model of the Leidenfrost state (cf. Ref. [16], where a more elaborate model was introduced in the same spirit).

The dense high packing fraction region at the top acts as a solid plug with a total mass  $M_{\text{plug}}$ , while the gaseous region below is equivalent to a spring, which applies a force to the plug that is proportional to its compression. Once the spring constant  $k$  is known, the frequency of oscillation of the spring is obtained from the force balance  $M_{\text{plug}}\ddot{u} = -ku$ , where  $u$  is the vertical displacement of the plug with respect to its equilibrium position. This leads to the well-known relation  $f_{\text{LFO}} = 1/\sqrt{2\pi} \sqrt{k/M_{\text{plug}}}$ .

To estimate  $k$  we use the fact that in steady state the pressure of the plug  $P_{\text{plug}}$  must be equal to the pressure  $P_{\text{gas}}$  in the gaseous region just below the plug

$$P_{\text{gas}} = P_{\text{plug}} = \frac{gM_{\text{plug}}}{L^2}, \quad (4)$$

where  $L^2$  is the bottom area of the container. Using the (admittedly bold) assumption that the gaseous region is compressed in accordance with Boyle's law for ideal gases, we write  $V_{\text{gas}}\Delta P_{\text{gas}} = -P_{\text{gas}}\Delta V_{\text{gas}}$ , where the equilibrium gas volume  $V_{\text{gas}}$  is the typical height  $\lambda$  times the bottom area of the container  $L^2$ , the differential volume can be written as  $\Delta V_{\text{gas}} = uL^2$ , and the differential gas pressure  $\Delta P_{\text{gas}}$  is written as the differential gas force per area  $\Delta F_{\text{gas}}/L^2$ . This leads to

$$\Delta F_{\text{gas}} = -\left(\frac{gM_{\text{plug}}}{\lambda}\right)u, \quad (5)$$

which is recognized as the force term in the equation for an harmonic oscillator with  $k = gM_{\text{plug}}/\lambda$ .

The size of the gaseous region is proportional to the typical kinetic energy gain of a particle when colliding with the bottom and gravity, i.e.,  $\lambda \sim T_0/g$ . The granular temperature  $T_0$  will be set by the temperature of the vibrating bottom  $T_0 \sim a_0^2 f_0^2$ . This linear relation is verified using numerical simulations, as shown in Fig. 7(a), where the granular temperature  $T$  is calculated as the average temperature of the whole system [28]. Inserting this approximation in the above expressions for  $k$  and

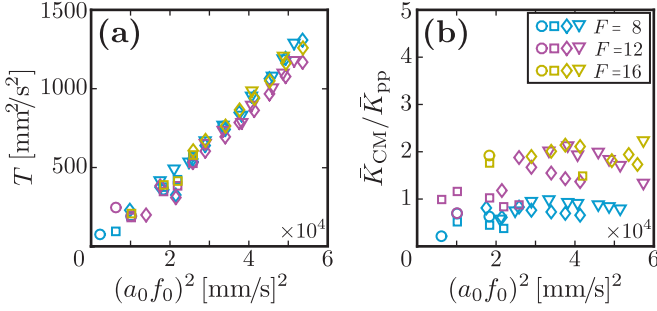


FIG. 7. (a) The granular temperature  $T$  and (b) the ratio of the kinetic energy of the center of mass  $z_{CM}$  to the kinetic energy per particle,  $\bar{K}_{CM}/\bar{K}_{PP}$ , are plotted versus  $(a_0 f_0)^2$  for different numbers of layers  $F$  and a constant particle diameter  $d = 1$  mm, both correspond to numerical simulation results. The different symbols correspond to different amplitudes of the shaker,  $\circ = 1.0$  mm,  $\square = 2.0$  mm,  $\diamond = 3.0$  mm,  $\nabla = 4$  mm.

$f_{LFO}$ , we find that  $M_{plug}$  cancels out and

$$f_{LFO} \sim \frac{g}{T_0^{1/2}} \sim \frac{g}{a_0 f_0} \Rightarrow \tilde{f}_{LFO} \equiv \frac{f_{LFO} a_0 f_0}{g}, \quad (6)$$

providing us with a natural frequency scale for the LFO which directly leads to the above definition of the dimensionless LFO frequency  $\tilde{f}_{LFO}$ .

The control parameter  $S_d$ , however, also requires some thought. In fact, the choice of the particle diameter  $d$  as a typical intrinsic length scale in Eq. (3) had so far been motivated by the fact that it was a convenient length scale which was kept fixed in the work in which it was introduced. Since we actually vary  $d$ , we are in need of a control parameter that better corresponds to the physics of the system we are studying. Let us therefore make a few assumptions about the granular Leidenfrost state. First, let us assume that the dissipation in the gaseous region is negligible in comparison with that in the dense region above it. This can be motivated from the fact that particles in the latter region are very close and therefore collisions very frequent. In a steady state, this means that the particles in the gaseous region are just transporting energy from the bottom to the plug, where it is subsequently dissipated. This is reminiscent of a famous work from the Kadanoff group [29,30] where a single particle transports energy from a hot wall to a granular cluster. Now, in our case suppose that a single particle picks up a kinetic energy  $\sim T_0 \sim a_0^2 f_0^2$  at the bottom. This energy needs to be dissipated in the plug, and since in height there are typically  $F$  particles to do so, the dissipated energy should scale as  $F^2 T_0 \sim (F a_0 f_0)^2$ . It is therefore plausible that for Leidenfrost states with a similar gaseous region (and therefore similar  $f_{LFO}$ ) we have the same value of  $F a_0 f_0$ . Nondimensionalizing the latter parameter with the velocity scale  $\sqrt{gL}$ , we obtain the following control parameter [31]

$$B = \frac{a_0 f_0 F}{\sqrt{gL}}. \quad (7)$$

In Fig. 8 the data of Fig. 6 are plotted using the new dimensionless parameters  $\tilde{f}_{LFO}$  and  $B$ . We see that all realized experiments and numerical simulations collapse onto a single curve. This collapse is in agreement with the observations of

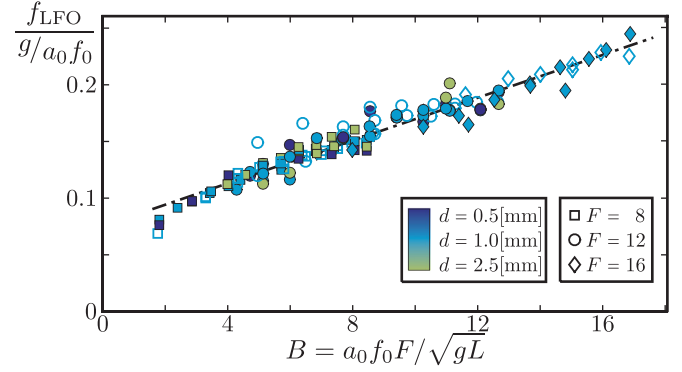


FIG. 8. The dimensionless frequency of the low-frequency oscillations  $\tilde{f}_{LFO}$  as a function of the shaking parameter  $B$  collapses all simulational data (as shown in Fig. 6) onto a single curve. Different symbols correspond to different numbers of layers  $F$  and different colors to different particle diameters  $d$ . As in Fig. 6, the solid symbols represent experimental data and the open symbols numerical simulation results. The dashed-dotted line serves as a guide to the eye.

Rivas *et al.* [16], where the container length  $L_x$  is varied and seen to have no influence on the normalized  $f_{LFO}$ , as long as the system stays in the Leidenfrost state.

### C. Time autocorrelation

Now that we qualitatively understand the physics behind the LFO, we turn our attention to the driving mechanism. When one identifies an oscillation it is namely not sufficient to identify the oscillating object itself; we must also know what keeps the oscillation going, e.g., a bow needs to be drawn across a violin string in order for the latter to produce sound. To answer this question, we note that the LFO is quasiperiodic rather than purely harmonic, i.e., it is not a clear periodic signal in time. Moreover it appears to be decoupled from the driving in the sense that for constant  $a_0 f_0$  the amplitude and frequency of the LFO are independent of  $a_0$  or, equivalently,  $f_0$  which can therefore be ruled out as the direct driving mechanism. We compute the autocorrelation function of the center of mass

$$\xi(t_0) = \frac{\langle z_{CM}(t+t_0)z_{CM}(t) \rangle_t}{\langle (z_{CM}(t))^2 \rangle_t}, \quad (8)$$

where  $\langle \dots \rangle_t$  indicates a time average. The result is shown in Fig. 9(a). Clearly, the autocorrelation function of the pure signal is dominated by the frequency of energy injection, which is the highest frequency present in the blue curve. Thus, the damped low-frequency oscillation that appears as a modulation of the high frequency signal is quite hard to recognize. We therefore choose to first low-pass filter the  $z_{CM}(t)$  signal, with a cutoff frequency  $f_c = f_{LFO} + (f_0 - f_{LFO})/2$ , that is, in between the frequencies of the LFO and the shaker. The autocorrelation function of the filtered signal accurately captures the autocorrelation on a larger timescale, as shown in Fig. 9(a). The location of the maxima and minima of  $\xi(t_0)$  are verified to correspond with the period  $\tau_{LFO} = 1/f_{LFO}$  of the LFO. Furthermore, we observe that the maxima (and minima) of  $\xi(t_0)$  decay exponentially in time. The corresponding typical decay timescale  $\tau$  is obtained by fitting the successive maxima to an exponential  $y(t_0) = e^{-t_0/\tau}$ , as shown in Fig. 9(b). This

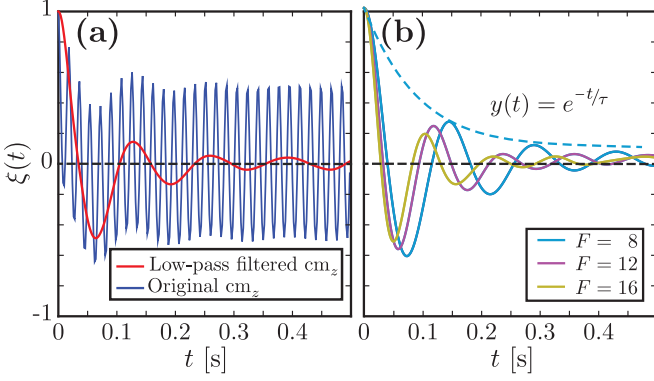


FIG. 9. (a) Autocorrelation function of the original center-of-mass signal  $z_{\text{CM}}(t)$  (blue line) and of the low-pass-filtered center of mass (red line) for  $a_0 = 4$  mm,  $f_0 = 55.7$  Hz,  $S_d = 200$ , and  $F = 12$ . (b) The autocorrelation function of the low-pass-filtered center-of-mass signal is plotted versus time for different number of layers and shaking strength  $S_d = 200$ . The dashed line represents the fit of the maxima for  $F = 8$ .

time decay can be readily interpreted as a decorrelation time, i.e., it is a measure for how fast the oscillating system loses phase information or, conversely, what the typical coherence time of the signal is.

The decorrelation time increases with  $S_d$ , as was suggested by the narrowing peaks of the spectra of  $z_{\text{CM}}(t)$  (Fig. 5). Moreover, we see that the correlation is inversely proportional to both  $d$  and  $F$ , suggesting that, in general, correlations are higher for systems with a higher number of particles, as seen in Fig. 10 for experimental and numerical data.

### D. Time scales

In the literature three different timescales have been identified in (dilute) vertically driven granular systems from hydrodynamic descriptions [17,19]. These three timescales are associated to the different processes that take place in a driven granular system. The first and fastest inertial timescale is associated to the mechanical response of the system and is identical to the one we introduced to nondimensionalize the LFO frequency, namely  $\tau_{\text{osc}} = a_0 f_0 / g$ . The second timescale is connected to heat conduction and was shown to be equal to  $\tau_{\text{heat}} = F a_0 f_0 / g$  and, finally, the third and largest timescale corresponds to dissipative processes and can be approximated as  $\tau_{\text{diss}} \sim a_0 f_0 / (g \varepsilon F)$ . Here the inelasticity coefficient  $\varepsilon = 1 - e^2$  is given in terms of the (nominal) normal coefficient of restitution  $e$ . Since, although unknown,  $\varepsilon$  can be assumed to be constant in the experiments conducted in this work, we just use  $\tau_d \equiv \sum \tau_{\text{diss}} = a_0 f_0 / (g F)$  as a reference timescale.

When the decorrelation time  $\tau$  is rescaled with  $\tau_d$  it is roughly independent of any parameter, as can be appreciated in Fig. 10(c), where the dimensionless decorrelation time  $\hat{\tau} \equiv \tau / \tau_d$  is plotted versus the shaking parameter  $B$ . Therefore,

$$\tau \sim \tau_d \sim \frac{a_0 f_0}{g F}, \quad (9)$$

which implies that the system becomes more coherent with increasing shaking strength (i.e., when  $a_0 f_0$  increases) and loses its coherency when the number of layers in the system

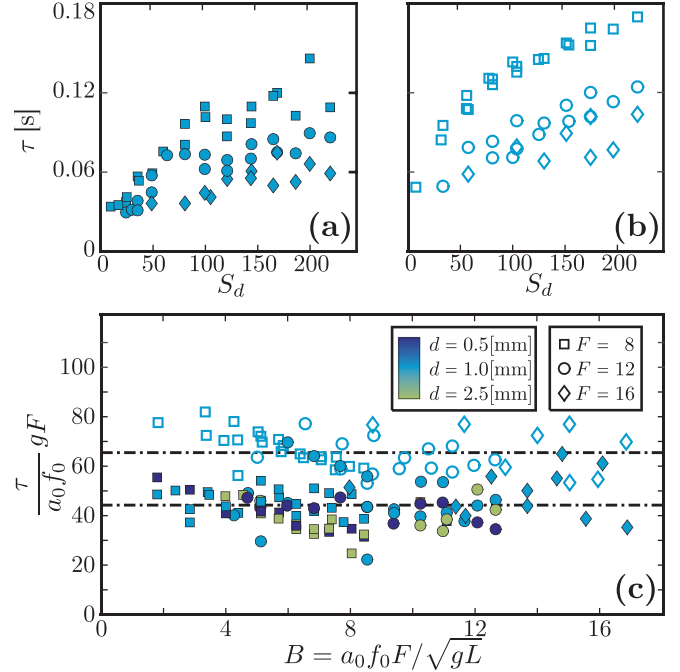


FIG. 10. Decorrelation time  $\tau$  determined from the autocorrelation function  $\xi(t_0)$  of the center of mass signal  $z_{\text{CM}}(t)$ . (a) Experimental data for  $\tau$  as a function of the dimensionless shaking strength  $S_d$  for different values of the number of layers  $F$  and the particle diameter  $d$  (see legend at the bottom). (b) Numerical data for  $\tau$ , again as function of  $S_d$ . (c)  $\tau$  nondimensionalized with the dissipative timescale  $\tau_d = a_0 f_0 / (g F)$  plotted versus the shaking parameter  $B$ . The horizontal lines correspond to the averaged value of  $\tau / \tau_d$  for the numerical simulations and the experiments. As in previous plots, different symbols correspond to different numbers of layers  $F$  and different colors to different particle diameters  $d$ , and the solid and open symbols represent experimental and numerical data, respectively.

$F$  increases. This is consistent with the view that the LFO is driven by the noise in the system, which increases with the driving strength  $a_0 f_0$  but decreases when the number of layers  $F$  in the system increases.

Note that the large value of the dimensionless decorrelation time ( $\tau / \tau_d \sim 50$ ), in both experiment and numerical simulations, is connected to the fact that  $\tau_d$  needs to be divided by the inelasticity  $\varepsilon$ , which is typically much smaller than 1, to obtain the dissipative timescale  $\tau_{\text{diss}}$ . In addition, the constant value of  $\tau / \tau_d$  is larger for numerical simulation than experimental data, which can be attributed to differences between simulation and experiment as, e.g., the role of particle-wall dissipation.

### E. LFO intensity

Finally, we turn to the strength of the oscillation by measuring the oscillation intensity  $I_{\text{LFO}}$ , namely the amplitude of the PSD at the oscillation frequency  $f_{\text{LFO}}$ . This quantity is plotted in Fig. 11 for (a) the experiments and (b) the numerical simulations as a function of the shaking strength  $S_d$ . We observe that  $I_{\text{LFO}}$  (for any fixed  $F$  and  $d$ ) increases with the shaking strength  $S_d$  and that there is a dramatic influence of the number of layers  $F$ , with  $I_{\text{LFO}}$  dropping quickly as a function of  $F$ .

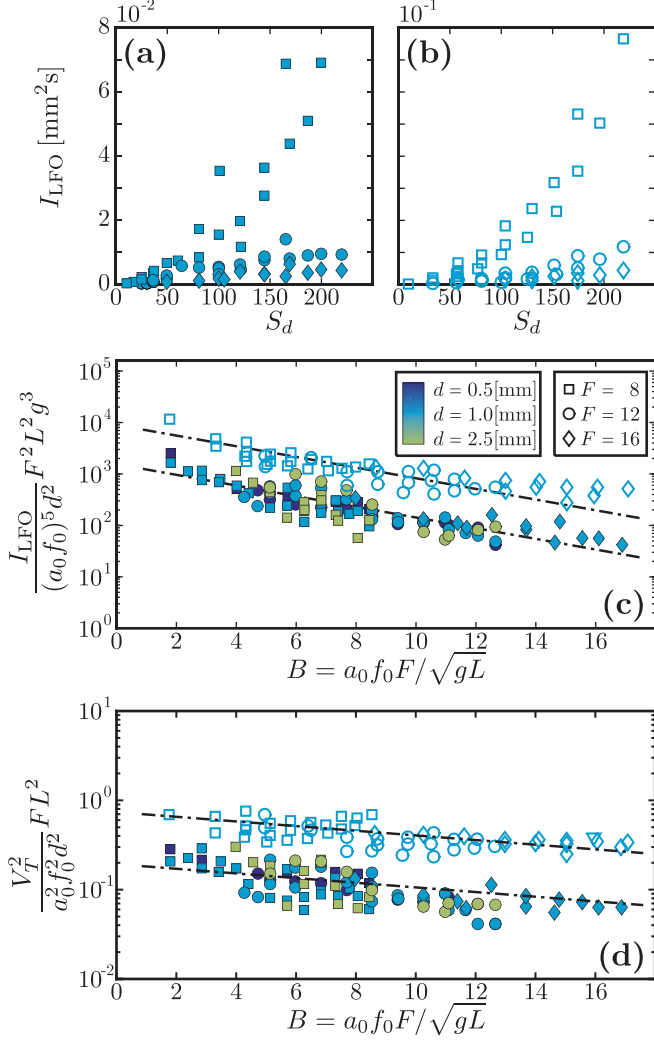


FIG. 11. Intensity  $I_{\text{LFO}}$  obtained from the PSD of the center-of-mass signal  $z_{\text{CM}}(t)$ . Top left: Experimental data for  $I_{\text{LFO}}$  as a function of the dimensionless shaking strength  $S_d$  for different values of the number of layers  $F$  and the particle diameter  $d$  (see legend at the bottom). Top right: Numerical data for  $I_{\text{LFO}}$ , again as function of  $S_d$ . Bottom:  $I_{\text{LFO}}$  nondimensionalized by  $(a_0 f_0)^5 d^2 / (L^2 g^3 F)$  plotted versus the shaking parameter  $B$ . The dashed-dotted line serves as a guide to the eye. As in previous plots, different symbols correspond to different numbers of layers  $F$ , different colors to different particle diameters  $d$ , and the solid and open symbols represent experimental and numerical data, respectively.

The shape of the PSD (Fig. 5) and the time-autocorrelation function (Fig. 8) suggests an approximate description in terms of a Langevin equation of a noise-driven harmonic oscillator (also known as Brownian motion in a harmonic potential) which is textbook material in nonequilibrium statistical mechanics [32],

$$\ddot{\zeta} = -\eta \dot{\zeta} - \omega_{\text{LFO}}^2 \zeta + \xi, \quad (10)$$

where  $\omega_{\text{LFO}} = 2\pi f_{\text{LFO}}$ ,  $\zeta(t) = z_{\text{CM}}(t) - \langle z_{\text{CM}} \rangle$  is the vertical deviation of the center-of-mass location from its time average  $\langle z_{\text{CM}} \rangle$ ,  $\eta = 2/\tau$  corresponds to twice the inverse decorrelation time, and  $\xi(t)$  is delta-correlated white noise, obeying a fluctuation-dissipation relation  $\langle \xi(t)\xi(t') \rangle = 2\eta V_T^2 \delta(t-t')$ .

Here  $V_T$  stands for the thermal velocity of the center of mass. In fact, such a Langevin approach had been suggested by Wakui and Isobe in Ref. [17], where a Langevin description of a dilute vibrated granular gas (i.e., without density inversion and the clearly observable Leidenfrost oscillation) was proposed.

The PSD  $S(\omega)$  corresponding to Langevin Eq. (10) is readily calculated theoretically [32]

$$S(\omega) = \frac{2\eta V_T^2}{[(\omega_{\text{LFO}}^2 - \omega^2)^2 + \eta^2 \omega^2]}. \quad (11)$$

Using the measured values for  $I_{\text{LFO}}$ ,  $f_{\text{LFO}}$ , and  $\tau$  we plot the above expression together with the experimental PSDs in Fig. 5 and find very good agreement for frequencies around and lower than the Leidenfrost oscillation frequency but also that Eq. (11) significantly underpredicts the participation of the higher frequencies in the experimental PSD.

Clearly, the numerator being constant,  $S(\omega)$  is maximum when the denominator obtains its smallest value, which gives:

$$I_{\text{LFO}} = \frac{2V_T^2}{\eta(\omega_{\text{LFO}}^2 - \frac{1}{4}\eta^2)} \approx \frac{\tau V_T^2}{\omega_{\text{LFO}}^2}, \quad (12)$$

where the last approximation originates from the expectation that  $\eta \ll \omega_{\text{LFO}}$ . The only quantity of which the scaling behavior is unknown is the thermal velocity of the center of mass,  $V_T$ .

Figure 7(b) shows the ratio of the kinetic energy of the center of mass  $z_{\text{CM}}$  to the kinetic energy per particle, i.e.,  $\bar{K}_{\text{CM}} = \bar{K}_{\text{pp}}$ , for the simulation data. It can be seen that there is an approximate equipartition of energy, i.e.,  $\bar{K}_{\text{CM}} \approx \bar{K}_{\text{pp}} \approx k_B T_0 \approx 1$ , and hence  $V_T$  is linked to the thermal velocity  $v_T \sim a_0 f_0$  of the grains by  $\frac{1}{2} M_{\text{tot}} V_T^2 \approx \frac{1}{2} m v_T^2$ , with the total mass  $M_{\text{tot}} = Nm$  given by the product of the number of particles  $N$  and the grain mass  $m$ . This leads to

$$V_T^2 \approx \frac{m}{M_{\text{tot}}} v_T^2 \sim \frac{a_0^2 f_0^2}{N}. \quad (13)$$

Using the above result with the previously corroborated  $\tau \sim a_0 f_0 / (gF)$  and  $\omega_{\text{LFO}} \sim g / (a_0 f_0)$  provides the scaling

$$I_{\text{LFO}} \sim \frac{(a_0 f_0)^5}{g^3 F N} \sim \frac{(a_0 f_0)^5 d^2}{g^3 F^2 L^2}, \quad (14)$$

where in the last step we have used that  $N = FL^2/d^2$ . In Fig. 11(c) we rescale  $I_{\text{LFO}}$  with the right-hand side of Eq. (14) and plot it as a function of the shaking parameter  $B$  and find a fair data collapse for both the experimental and the numerical data. Moreover, it can be seen that the dimensionless  $I_{\text{LFO}}$  data decay exponentially with  $B$ . Since  $\hat{\tau}$  is approximately constant and  $f_{\text{LFO}}$  has nonexponential behavior (Fig. 7 suggests that it increases as a power law of  $B$ ), this exponential decay appears to be connected to the violation of energy equipartition, as might be anticipated for this far-from-equilibrium system. More specifically, we find that the ratio of the thermal energy of the center of mass and that of the particles decays exponentially, i.e.,

$$V_T^2 = 4\pi^2 \frac{a_0^2 f_0^2}{N} \phi(B), \quad (15)$$

where  $\phi(B)$  is an exponentially decaying function of the shaking parameter  $B$ .

To test the above, we use Eq. (12) to express  $V_T^2$  in terms of the measured quantities  $I_{\text{LFO}}$ ,  $f_{\text{LFO}}$ , and  $\tau$  and subsequently nondimensionalize with  $a_0^2 f_0^2 / N$  and obtain the result plotted in Fig. 11(d), which corroborates our expectation: There indeed appears to be an exponential decay of the ratio of the thermal energy of the center of mass and that of the particles. There are many probable causes why energy equipartition may deteriorate for larger  $B$ . The most obvious one is dissipation, which makes it unlikely for the thermal energy of the gas particles and that of the plug to be equilibrated. A more subtle effect is that the plug is not a fixed entity moving as a Brownian particle but itself consists of many particles that will respond to collisions with the particles in the gaseous layer. This will lead to the observed much stronger participation of the higher frequencies in the PSD than expected based on the simple Langevin model Eq. (10). And a stronger participation of the higher frequencies directly implies a lower intensity at the resonance frequency  $f_{\text{LFO}}$ , even if there would be equipartition.

#### IV. CONCLUSIONS

We have experimentally and numerically studied the LFO in a vibrated quasi-one-dimensional column of granular material in the Leidenfrost state. This LFO manifests itself as a vertical oscillation of the dense top layer of the Leidenfrost state. We determined the LFO frequency from the power spectral density of the center-of-mass signal for different amplitude

and frequency of the driving, particle diameters, and number of layers in the system.

In search of scaling laws, we constructed a simplified mass-spring model of the Leidenfrost state and argued that the LFO frequency should be inversely proportional to the fast inertial timescale, which is independent of the particle diameter and the number of layers. The dimensionless oscillation frequency is found to depend on the shaking parameter  $B = a_0 f_0 F / \sqrt{gL}$ , which was motivated qualitatively from the balance of energy input and dissipation in the dense layer. Experimental and numerical results are in fair agreement with each other.

Subsequently, we studied the time autocorrelation function of the center-of-mass signal and found that the LFO decorrelates with a typical decay time  $\tau$ , which was found to be proportional to the dissipative timescale  $\tau_{\text{diss}} = a_0 f_0 / (gF)$  and otherwise independent of any other parameter in the system. Such a decorrelation is consistent with the view that the LFO is driven by the inherent noise in the system, which increases with the driving strength  $a_0 f_0$  but decreases with the number of layers  $F$ .

Finally, we argue that the vertical position of the center of mass can be approximately described by a Langevin equation with weak white noise. We find that the amplitude of the oscillation, measured as the oscillation intensity in the PSD, scales consistently with that expected from the Langevin description. We find that energy equipartition is violated in this far-from-equilibrium system and that the portion of energy partitioned with the oscillating dense top layer is decaying significantly with increasing shaking strength.

- 
- [1] H. M. Jaeger, S. R. Nagel, and R. P. Behringer, The physics of granular materials, *Phys. Today* **49**(4), 32 (2008).
  - [2] P. Eshuis, K. V. D. Weele, D. van der Meer, R. Bos, and D. Lohse, Phase diagram of vertically shaken granular matter, *Phys. Fluids* **19**, 123301 (2007).
  - [3] S. Douady, S. Fauve, and C. Laroche, Subharmonic instabilities and effects in a granular layer under vertical vibrations, *Europhys. Lett.* **8**, 621 (1989).
  - [4] E. Clement, L. Labous, and L. Vanel, Granular packing under vibration, *Europhys. News* **29**, 107 (1998).
  - [5] O. Sano, Dilatancy, buckling, and undulations on a vertically vibrating granular layer, *Phys. Rev. E* **72**, 051302 (2005).
  - [6] F. Melo, P. Umbanhowar, and H. L. Swinney, Transition to Parametric Wave Patterns in a Vertically Oscillated Granular Layer, *Phys. Rev. Lett.* **72**, 172 (1994).
  - [7] S. J. Moon, M. D. Shattuck, C. Bizon, D. I. Goldman, J. B. Swift, and H. L. Swinney, Phase bubbles and spatiotemporal chaos in granular patterns, *Phys. Rev. E* **65**, 011301 (2001).
  - [8] M. Faraday, On a peculiar class of acoustical figures; and on certain forms assumed by groups of particles upon vibrating elastic surfaces, *Philos. Trans. R. Soc. Lond.* **121**, 299 (1831).
  - [9] M. C. Cross and P. C. Hohenberg, Pattern formation outside of equilibrium, *Rev. Mod. Phys.* **65**, 851 (1993).
  - [10] P. Eshuis, K. van der Weele, D. van der Meer, and D. Lohse, Granular Leidenfrost Effect: Experiment and Theory of Floating Particle Clusters, *Phys. Rev. Lett.* **95**, 258001 (2005).
  - [11] E. W. C. Lim, Granular Leidenfrost effect in vibrated beds with bumpy surfaces, *Eur. Phys. J. E: Soft Matter* **32**, 365 (2010).
  - [12] K. Roeller and S. Herminghaus, Dynamics of the wet granular Leidenfrost phenomenon, *Phys. Rev. E* **86**, 021301 (2012).
  - [13] J. G. Leidenfrost, *De aquae communis nonnullis qualitatibus tractatus* (Ovenius, 1756).
  - [14] S. Chandrasekhar, *Hydrodynamic and Hydromagnetic Stability* (Dover, London, 1961).
  - [15] D. Paolotti, A. Barrat, U. Marini, B. Marconi, and A. Puglisi, Thermal convection in monodisperse and bidisperse granular gases: A simulation study, *Phys. Rev. E* **69**, 061304 (2004).
  - [16] N. Rivas, S. Luding, and A. R. Thornton, Low-frequency oscillations in narrow vibrated granular systems, *New J. Phys.* **15**, 113043 (2013).
  - [17] J. Wakou and M. Isobe, Fluctuation-dissipation relations for motions of center of mass in driven granular fluids under gravity, *Phys. Rev. E* **85**, 061311 (2012).
  - [18] C. R. K. Windows-Yule, N. Rivas, D. J. Parker, and A. R. Thornton, Low-frequency oscillations and convective phenomena in a density-inverted vibrofluidized granular system, *Phys. Rev. E* **90**, 062205 (2014).
  - [19] Y. Bromberg, E. Livne, and B. Meerson, Development of a density inversion in driven granular gases, in *Granular Gas Dynamics*, Lecture Notes in Physics Vol. 624 (Springer, Berlin, 2003), pp. 251–266.
  - [20] B. D. Lubachevsky, How to simulate billiards and similar systems, *J. Comput. Phys.* **94**, 255 (1991).



- [21] S. McNamara and E. Falcon, Simulations of vibrated granular medium with impact-velocity-dependent restitution coefficient, *Phys. Rev. E* **71**, 031302 (2005).
- [22] T. Poschel, N. V. Brilliantov, and T. Schwager, Long-time behavior of granular gases with impact-velocity dependent coefficient of restitution, *Physica A* **325**, 274 (2003).
- [23] H. K. Pak and R. P. Behringer, Surface Waves in Vertically Vibrated Granular Materials, *Phys. Rev. Lett.* **71**, 1832 (1993).
- [24] D. Serero, N. Gunkelmann, and T. Poschel, Hydrodynamics of binary mixtures of granular gases with stochastic coefficient of restitution, *J. Fluid Mech.* **781**, 595 (2015).
- [25] N. Gunkelmann, M. Montaine, and T. Poschel, Stochastic behavior of the coefficient of normal restitution, *Phys. Rev. E* **89**, 022205 (2014).
- [26] N. Gunkelmann, D. Serero, and T. Poschel, Temperature of a granular gas with regard to the stochastic nature of particle interactions, *New J. Phys.* **15**, 093030 (2013).
- [27] G. Castillo, N. Mujica, and R. Soto, Fluctuations and Criticality of a Granular Solid-Liquid-Like Phase Transition, *Phys. Rev. Lett.* **109**, 095701 (2012).
- [28] We chose to represent the temperature in the whole system, rather than only that of the gaseous region, to avoid having to add a—rather arbitrary—cut off between the two regions.
- [29] Y. Du, H. Li, and L. P. Kadanoff, Breakdown of Hydrodynamics in a One-Dimensional System of Inelastic Particles, *Phys. Rev. Lett.* **74**, 1268 (1995).
- [30] P. Eshuis, K. van der Weele, E. Calzavarini, D. Lohse, and D. van der Meer, Exploring the limits of granular hydrodynamics: A horizontal array of inelastic particles, *Phys. Rev. E* **80**, 011302 (2009).
- [31] Note that this velocity scale has been chosen for convenience since the bottom dimensions  $L$  are not varied in this experiment. One might equally well have chosen any other fixed length scale, such as a reference particle diameter.
- [32] R. Zwanzig, *Nonequilibrium Statistical Mechanics* (Oxford University Press, Oxford, 2001).